Square lattice hard-core bosons within the random phase approximation

T. N. Antsygina, M. I. Poltavskaya, I. I. Poltavsky, and K. A. Chishko
B. Verkin Institute for Low Temperature Physics and Engineering, 61103 Kharkov, Ukraine
(Received 2 July 2009; revised manuscript received 8 October 2009; published 10 November 2009)

Using random phase approximation we build finite-temperature phase diagrams and calculate thermodynamic functions of a square lattice hard-core boson model with nearest (nn) and next-nearest-neighbor (nnn) interactions in terms of equivalent to it an anisotropic spin-1/2 *XXZ* model in a magnetic field. The system undergoes liquid-solid phase transitions that can be either of the first or second order. Depending on the hopping value and ratio between nn and nnn interactions the system displays two types of critical behavior. The line of the first-order transitions terminates in a bicritical end point inside the solid phase or ends in a tricritical point continuously giving way to the second-order phase transition line. The connection of the hopping and the ratio between the nn and nnn interactions with criticality of the system is investigated. The critical line separating the regions of specific critical behavior is built. Reentrant liquid-solid-liquid phase transitions are found and discussed.

DOI: 10.1103/PhysRevB.80.174511 PACS number(s): 64.70.Tg, 75.40.Cx

I. INTRODUCTION

A hard-core boson (HCB) concept[1–3] as a version of a quantum lattice gas model is widely used for different scientific applications.[4–14] The model is appropriate for the description of quantum condensed systems such as atomic and molecular monolayers on substrates of different kinds[15,16] and particles trapped in optical lattices.[10,17–19] It is also used in helium physics, supersolid phenomena, and superconductivity. The HCB Hamiltonian is naturally mapped into an anisotropic spin-1/2 *XXZ* model in a magnetic field, one of the central models of the quantum magnetism, whose properties are in itself of great interest.

A hard-core boson model on a square lattice is known to exemplify liquid, solid, and superfluid phases. Finite-temperature phase diagrams for classical and quantum square lattice HCB models have been investigated for the most part numerically.[20–28] Analytically the diagrams were built mainly within mean field approximation (MFA),[29,30] which in essence implies that the Ising model was treated, so that the hopping term in the HCB Hamiltonian was completely neglected. These investigations showed that the system undergoes liquid-solid transitions which can be either of the first or second order and displays bicritical or tricritical behavior.

It is important to elucidate using analytical methods how the hopping modifies the properties of the HCB system as compared with those found within MFA. For this, in the present paper using two-time Green-function formalism with the decoupling on the first step[31] (random phase approximation) we build finite-temperature phase diagrams and calculate thermodynamic functions for a quantum square lattice hard-core boson model with nearest-neighbor (nn) and next-nearest-neighbor (nnn) interactions. The main goal is to find out effect of the hopping on the topology of the liquid—Néel solid phase diagrams and to investigate how the hopping and the ratio between nn and nnn interactions affect the type of critical behavior. The nn interaction is assumed to be repulsive while nnn interaction is considered to be either attractive or moderately repulsive, so that the striped (collinear) or other complicated phases appearing at high nnn repulsion are beyond the scope of the present paper. This assumption is quite realistic when we consider real systems such as monolayers on substrates[15,16] or particles in optical lattices.[10,17–19]

The paper is organized as follows. In Sec. II we present the HCB Hamiltonian and its magnetic analog. In Sec. III we outline the mean-field results for the system under study. In this and subsequent sections analytical calculations are made for the magnetic system. In Sec. IV we determine the random-phase approximation (RPA) finite-temperature phase diagrams at various values of the parameters and discuss the obtained results using both magnetic and HCB languages. In Sec. V using RPA we calculate thermodynamic functions such as the internal energy, heat capacity, and magnetic susceptibility. Conclusions are presented in Sec. VI.

II. HAMILTONIAN

The Hamiltonian of the hard-core bosons is

$$H_B = -\frac{t}{2}\sum_{\mathbf{f},\boldsymbol{\delta}} (a^+_{\mathbf{f}} a_{\mathbf{f}+\boldsymbol{\delta}} + a^+_{\mathbf{f}+\boldsymbol{\delta}} a_{\mathbf{f}}) + \frac{V_1}{2}\sum_{\mathbf{f},\boldsymbol{\delta}} n_{\mathbf{f}} n_{\mathbf{f}+\boldsymbol{\delta}} - \frac{V_2}{2}\sum_{\mathbf{f},\boldsymbol{\gamma}} n_{\mathbf{f}} n_{\mathbf{f}+\boldsymbol{\gamma}} - \mu\sum_{\mathbf{f}} n_{\mathbf{f}}, \quad (1)$$

where t is the nearest-neighbor hopping, $V_{1,2}$ are the interparticle interactions, $\boldsymbol{\delta}$ ($\boldsymbol{\gamma}$) is the vector connecting nn (nnn), μ is the chemical potential, $a^+_{\mathbf{f}}$ and $a_{\mathbf{f}}$ are the Pauli creation and annihilation operators of a hard-core boson at site $\mathbf{f}$, satisfying the following commutation relations:

$$[a^+_{\mathbf{f}}, a^+_{\mathbf{g}}] = [a_{\mathbf{f}}, a_{\mathbf{g}}] = [a_{\mathbf{f}}, a^+_{\mathbf{g}}] = 0 \quad (\mathbf{f} \neq \mathbf{g}),$$

$$[a^+_{\mathbf{f}}, a^+_{\mathbf{f}}]_+ = [a_{\mathbf{f}}, a_{\mathbf{f}}]_+ = 0, \quad [a_{\mathbf{f}}, a^+_{\mathbf{f}}]_+ = 1,$$

so that the double occupation of a lattice site is forbidden, and the occupation number $n_{\mathbf{f}} = a^+_{\mathbf{f}} a_{\mathbf{f}}$ is equal either 1 or 0. In our consideration V_1 is always positive while V_2 can be positive or negative.

This model is equivalent to a 1/2-spin *XXZ* magnet. A down spin corresponds to an occupied site, while an up spin corresponds to an empty site,[2]

$$a_{\mathbf{f}}^{+} \to S_{\mathbf{f}}^{-}, \quad a_{\mathbf{f}} \to S_{\mathbf{f}}^{+}, \quad n_{\mathbf{f}} \to \frac{1}{2} - S_{\mathbf{f}}^{z}. \tag{2}$$

Substituting Eq. (2) into Hamiltonian (1), we get

$$H_B = H_M - NE_0,$$

where H_M is the Hamiltonian of an anisotropic XXZ model,

$$H_M = -\frac{J}{2}\sum_{\mathbf{f},\boldsymbol{\delta}} (S_{\mathbf{f}}^{+}S_{\mathbf{f}+\boldsymbol{\delta}}^{-} - \Delta S_{\mathbf{f}}^{z}S_{\mathbf{f}+\boldsymbol{\delta}}^{z}) - \frac{J\alpha\Delta}{2}\sum_{\mathbf{f},\boldsymbol{\gamma}} S_{\mathbf{f}}^{z}S_{\mathbf{f}+\boldsymbol{\gamma}}^{z} - \mathcal{H}\sum_{\mathbf{f}} S_{\mathbf{f}}^{z}, \tag{3}$$

with a ferromagnetic transverse exchange $J=2t$. A longitudinal exchange for nn is antiferromagnetic and equal to $J\Delta$. The nnn exchange $J\alpha\Delta$ can be either ferro or antiferromagnetic, $\Delta=V_1/2t$, $\alpha=V_2/V_1$, and $\mathcal{H}=-\mu+\gamma_0(V_1-V_2)/2$ is an external magnetic field, $\gamma_0=4$ is a number of nn (nnn) for a square lattice, $E_0=[\mu-\gamma_0(V_1-V_2)/4]/2$, N is the total number of lattice sites. At $\alpha=0$ Hamiltonian (3) reduces to an anisotropic Heisenberg model. We consider the case when an inequality $2t<V_1+V_2$ $(\Delta(1+\alpha)>1)$ is satisfied. All the below calculations are valid for both signs of α. However, the range of $\alpha<-0.5$ when the striped (collinear) or other complicated phases can emerge[11,12,28] is not relevant to the purpose of the present paper.

III. MEAN-FIELD APPROXIMATION

Before proceeding to phase diagrams in the random phase approximation, we outline briefly the results for the system under study in the mean-field approximation. In the standard way, we divide the square lattice into two sublattices, A and B, and introduce the average sublattice magnetizations,

$$\langle S^z\rangle_A = \eta - \xi, \quad \langle S^z\rangle_B = \eta + \xi,$$

where η and ξ are the total and staggered magnetization per site. In the HCB terms the sublattice particle densities ρ_A and ρ_B and the average lattice coverage ρ are

$$\rho_{A(B)} = \frac{1}{2} - \langle S^z\rangle_{A(B)}, \quad \rho = \frac{1}{2} - \eta.$$

Hereafter all energy quantities are expressed in terms of $J\gamma_0\Delta$ so that

$$\theta = \frac{T}{J\gamma_0\Delta}, \quad h = \frac{\mathcal{H}}{J\gamma_0\Delta}.$$

The free energy of the anisotropic XXZ model (3) has the form

$$\frac{F_M}{N} = -\frac{1}{2}[(1-\alpha)\eta^2 - (1+\alpha)\xi^2] - \frac{\theta}{2}\left[\ln\left(2\cosh\frac{\omega_+}{2\theta}\right) + \ln\left(2\cosh\frac{\omega_-}{2\theta}\right)\right], \tag{4}$$

where

$$\omega_{\pm} = \omega_0 \pm (1+\alpha)\xi, \quad \omega_0 = h - (1-\alpha)\eta.$$

Minimizing the free energy (4) with respect to η and ξ, one gets the system of equations for η and ξ,

$$\eta + \xi = \frac{1}{2}\tanh\frac{\omega_+}{2\theta}, \quad \eta - \xi = \frac{1}{2}\tanh\frac{\omega_-}{2\theta}. \tag{5}$$

At $h=0$ the total magnetization $\eta=0$ at any temperature. The staggered magnetization ξ is nonzero only below the critical temperature $\theta_c^{MFA}=(1+\alpha)/4$. At $h\neq 0$ the magnetization $\eta \neq 0$, and there exist temperature and field ranges where ξ is also nonzero. A nontrivial solution η, $\xi\neq 0$ describes the state with different sublattice magnetizations, so that the system has a diagonal long-range order (DLRO). In the HCB model it corresponds to the solid phase defined as the state with nonequal sublattice particle densities $\rho_A \neq \rho_B$. With increase in field or temperature the system loses DLRO and turns into a paramagnetic state $(\xi=0)$ or, in the HCB language, into liquid.

It is known[30] that the liquid-solid (paramagnetic-antiferromagnetic) transitions can be either of the first or second order. Depending on the value of the parameter α the system can demonstrate different types of critical behavior.[21,30] The equation for the second-order transition line has the form[30]

$$h = \frac{1+\alpha}{4}\tau\ln\frac{1+\sqrt{1-\tau}}{1-\sqrt{1-\tau}} + \frac{1-\alpha}{2}\sqrt{1-\tau}, \tag{6}$$

where the normalized temperature $\tau=\theta/\theta_c^{MFA}$.

Now we derive the equation for the spinodal, the locus of critical points, that restricts the region with $\partial\eta/\partial h<0$ on the $\eta-\theta$ diagram. For this we employ the following condition:

$$\begin{Vmatrix} \frac{\partial^2 F_M}{\partial\eta^2} & \frac{\partial^2 F_M}{\partial\eta\,\partial\xi} \\ \frac{\partial^2 F_M}{\partial\xi\,\partial\eta} & \frac{\partial^2 F_M}{\partial\xi^2} \end{Vmatrix} = 0. \tag{7}$$

Substituting Eq. (4) into Eq. (7) with accounting for Eq. (5), we get

$$1 - (1-\alpha^2)P_+P_- - \alpha(P_+ + P_-) = 0,$$

$$P_{\pm} = \frac{1}{4\theta}[1 - 4(\eta \pm \xi)^2]. \tag{8}$$

After some manipulations Eq. (8) reduces to an equation for ξ as a function of temperature

$$\Lambda - \alpha\tilde{\tau} - 4\xi\coth\frac{4\xi}{\tau} = 0, \tag{9}$$

where the following notifications have been introduced

$$\Lambda = \sqrt{\tilde{\tau}^2 + 16\xi^2(1+\alpha\tilde{\tau})}, \quad \tilde{\tau} = \frac{\tau}{1-\alpha}.$$

The parameter η along the spinodal has the form

$$\eta = \frac{1}{2}\sqrt{1 + \alpha\tilde{\tau} + 4\xi^2 - \Lambda}, \tag{10}$$

and the magnetic field h as it follows from Eq. (5) can be written through ξ and η as

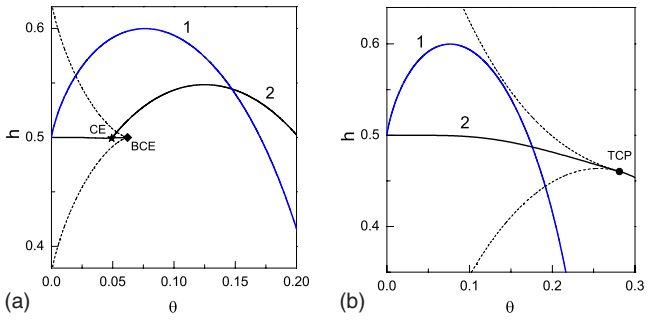

FIG. 1. (Color online) $h-\theta$ phase diagrams at: (a) $\alpha=0$ (1) and 0.25 (2) and (b) $\alpha=0$ (1) and 0.85 (2). Solid curves correspond to the equilibrium phase transition lines and the dashed ones to the spinodals. Full circle, diamond, and star denote the tricritical point, bicritical end point, and critical end point, respectively.

$$h=(1-\alpha)\eta-(1+\alpha)\xi+\frac{1+\alpha}{4}\tau\ln\frac{1+2(\eta+\xi)}{1-2(\eta+\xi)}. \quad (11)$$

The set of Eqs. (5), (6), and (9)–(11) enables one to build $h-\theta$ and $\eta-\theta$ phase diagrams within MFA. The lines of equilibrium first order phase transitions can be found using Eqs. (4) and (5).

The $h-\theta$ phase diagrams are shown in Fig. 1. Under and above the equilibrium phase transition lines there are the antiferromagnetic (solid) and paramagnetic (liquid) phases, correspondingly. It is seen that the topology of the diagrams depends significantly on α. Note, that Eq. (9) has a trivial solution $\xi=0$ for all α. If $-0.5<\alpha\leq 0$ this solution is the unique root of Eq. (9) so that at nonpositive α antiferromagnetic-paramagnetic (solid-liquid) transformations can be only of the second order (curve 1). For positive α Eq. (9) besides trivial has also nontrivial solutions: two at $0<\alpha<\alpha_c=0.6$ and one at $\alpha\geq\alpha_c$. Substituting these nontrivial solutions sequentially into Eqs. (10) and (11), we obtain the spinodals on the $\eta-\theta$ and $h-\theta$ diagrams. Thus, at positive α the first-order phase transitions appear in the system. At $0<\alpha<\alpha_c$ two nontrivial solutions of Eq. (9) determine two spinodal branches which terminate in a bicritical end point (BCE). The system displays the bicritical behavior [curve 2 in Fig. 1(a)] when at low temperatures up to a critical end point (CE) the solid-liquid phase transitions are of the first order while starting from θ_{CE} they are of the second order. A particular feature of this regime is that the first-order transition line extends into the solid phase ending inside it in the bicritical end point, so that in the temperature range $\theta_{\mathrm{CE}}<\theta<\theta_{\mathrm{BCE}}$ two solid phases with different densities coexist. If $\alpha=\alpha_c$ critical and bicritical points run into one tricritical point (TCP) and at $\alpha\geq\alpha_c$ the system demonstrates the tricritical behavior [curve 2 in Fig. 1(b)] when the first order phase transition line changes continuously into the second order one in TCP. In this case the only nontrivial solution of Eq. (9) specifies the upper spinodal branch that ends in TCP, whereas another spinodal branch is due to the trivial solution $\xi=0$. In the tricritical regime the solid exists only as a homogeneous phase.

The dependences of the normalized tricritical τ_{TCP} and bicritical τ_{BCE} temperatures on the parameter α as well as the quantity α_c can be found by simultaneous solution of Eq. (9) and the equation

$$\alpha-\frac{\tilde{\tau}}{\Lambda}+(1-\alpha)\left[\frac{4\xi/\tau}{\sinh(4\xi/\tau)}\right]^2=0,$$

which implies that the derivative of the left hand side of Eq. (9) with respect to ξ is equal to zero. In view of Eq. (9) the latter equation reduces to a quadratic one in $y=16\alpha\xi^2$,

$$(1+\alpha\tilde{\tau})y^2+Ay+B=0, \quad (12)$$

where

$$A=(1+\alpha\tilde{\tau})[\tilde{\tau}(3+2\alpha-4\alpha^2)-4\alpha]-\tilde{\tau},$$

$$B=(1+\alpha)\tilde{\tau}^2[1-3\alpha(1-\tau)].$$

The condition $\xi=0$ leads to $B=0$ which gives the TCP temperature as a function of α

$$\tau_{\mathrm{TCP}}=1-\frac{1}{3\alpha}, \quad (13)$$

whereas $A=0$ together with Eq. (13) gives $\alpha_c=0.6$. These results coincide with those reported in Ref. 30. The temperature τ_{BCE} can be found by a numerical solution of the set of Eqs. (9) and (12). It is interesting to note that at least for $0\leq\alpha\leq 0.3$

$$\tau_{\mathrm{BCE}}=\frac{\alpha}{1+\alpha}$$

to a high degree of accuracy.

IV. RPA FINITE-TEMPERATURE PHASE DIAGRAMS

Now we proceed to the solution of the problem within RPA. Writing down equations of motion for retarded commutator single-particle transverse Green functions with the decoupling on the first step[31] and making the Fourier transformation in them, we obtain

$$\left\{\omega-\omega_0+(1+\alpha)\xi\sigma_z-(\eta\sigma_x-i\xi\sigma_y)\frac{\Gamma_{\mathbf{k}}}{\Delta}\right\}\hat{G}=\frac{\eta-\xi\sigma_z}{\pi}, \quad (14)$$

where σ_ν $(\nu=x,y,z)$ are the Pauli matrices,

$$\hat{G}=\begin{pmatrix}G_{\mathbf{k}}^{AA} & G_{\mathbf{k}}^{AB}\\ G_{\mathbf{k}}^{BA} & G_{\mathbf{k}}^{BB}\end{pmatrix},$$

and the structure factor $\Gamma_{\mathbf{k}}$ is defined as

$$\Gamma_{\mathbf{k}}=\frac{1}{\gamma_0}\sum_{\boldsymbol{\delta}}\exp(i\mathbf{k}\boldsymbol{\delta}).$$

Solving Eq. (14), we get

$$G_{\mathbf{k}}^{AA}=\frac{\eta-\xi}{2\pi}\left(\frac{1-p}{\omega-\Omega_+}+\frac{1+p}{\omega-\Omega_-}\right), \quad (15)$$

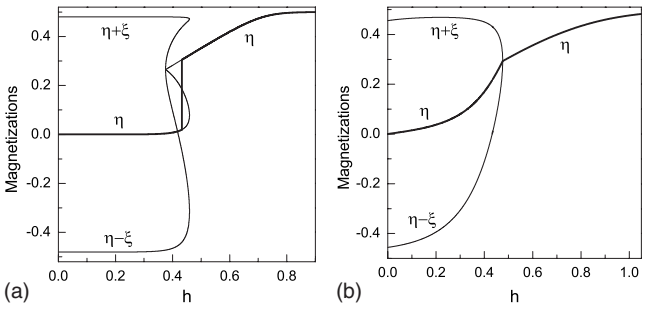

FIG. 2. Field dependences of total and sublattice magnetizations at $\Delta=1.5$, $\alpha=0.25$: (a) $\theta=0.04$ and (b) $\theta=0.15$.

$$G_{\mathbf{k}}^{AB}=-\frac{\eta^2-\xi^2}{2\pi}\frac{\Gamma_{\mathbf{k}}}{R\Delta}\left(\frac{1}{\omega-\Omega_+}-\frac{1}{\omega-\Omega_-}\right), \tag{16}$$

where

$$p=(1+\alpha)\frac{\xi}{R},\quad \Omega_\pm=\omega_0\pm R, \tag{17}$$

$$R=\sqrt{(1+\alpha)^2\xi^2+(\eta^2-\xi^2)\frac{\Gamma_{\mathbf{k}}^2}{\Delta^2}}. \tag{18}$$

Function G^{BB} can be obtained from G^{AA} by replacement $\xi\to-\xi$ and $G^{BA}=G^{AB}$. From Eq. (18) it follows that the approximation used here is valid for $\Delta(1+\alpha)>1$.

With the help of Eq. (15) we obtain the following set of equations for parameters η and ξ:

$$\frac{2(\eta+\xi)}{N}\sum_{\mathbf{k}}\left[(1+p)\coth\frac{\Omega_+}{2\theta}+(1-p)\coth\frac{\Omega_-}{2\theta}\right]=1,$$

$$\frac{2(\eta-\xi)}{N}\sum_{\mathbf{k}}\left[(1-p)\coth\frac{\Omega_+}{2\theta}+(1+p)\coth\frac{\Omega_-}{2\theta}\right]=1. \tag{19}$$

At zero field the total magnetization $\eta=0$ and the nonzero staggered magnetization ξ exists only below the critical temperature θ_c^{RPA} given by

$$(\theta_c^{RPA})^{-1}=\frac{8}{\pi(1+\alpha)}K\left(\frac{1}{\Delta(1+\alpha)}\right), \tag{20}$$

where $K(x)$ is the complete elliptic integral of the first kind. As it follows from Eq. (20), the critical temperature θ_c^{RPA} increases with α at fixed Δ and with Δ at fixed α.

Field dependences of the total and sublattice magnetizations obtained by solution of Eq. (19) are shown in Fig. 2 for two values of temperature. It is seen that depending on temperature a magnetic-field-induced phase transition from the antiferromagnetic into paramagnetic phase can be either of the (a) first or (b) second order. Since within RPA the free energy of the system cannot be calculated directly, we used the Maxwell equal area rule[32] to find the value of h corresponding to the equilibrium first-order phase transition in Fig. 2(a).

Now we calculate the finite-temperature phase diagrams for the system under study. The line of equal total and staggered magnetizations ($\xi=\eta$) can be found from an equation

$$1=\frac{8\theta}{\pi\lambda^2}K\left(\frac{1}{\Delta(1+\alpha)\lambda}\right),$$

$$\lambda^2=4\theta+(1+\alpha)\left[1-2h\coth\left(\frac{h(1+\alpha)}{2\theta}\right)\right].$$

The line of the second-order transitions results from Eq. (19) at $\xi\to0$ and is determined by the set of equations

$$\frac{2\eta}{N}\sum_{\mathbf{k}}\left(\coth\frac{\tilde{\Omega}_+}{2\theta}+\coth\frac{\tilde{\Omega}_-}{2\theta}\right)=1,$$

$$\frac{2\eta}{N}\sum_{\mathbf{k}}\frac{\Delta(1+\alpha)}{\Gamma_{\mathbf{k}}}\left(\coth\frac{\tilde{\Omega}_+}{2\theta}-\coth\frac{\tilde{\Omega}_-}{2\theta}\right)=-1,$$

where

$$\tilde{\Omega}_\pm=\omega_0\pm\eta\frac{\Gamma_{\mathbf{k}}}{\Delta}.$$

As to the first-order transitions, along with the equilibrium line we also calculate the spinodal which within RPA is defined from the condition that the derivatives $\partial\eta/\partial h\to\infty$ and $\partial\xi/\partial h\to\infty$ hold valid simultaneously. Note, that these conditions within MFA lead to the same result Eq. (8) as Eq. (7) does. The spinodal equation enables us to delimit the regions of different critical behaviors and to define the critical values of α and Δ where one critical regime changes the other. Differentiating Eq. (19) with respect to h, after some manipulations, we get

$$A(\eta,\xi)B(\eta,-\xi)+A(\eta,-\xi)B(\eta,\xi)=0. \tag{21}$$

Here the following notations have been introduced:

$$A(\eta,\xi)=1+\frac{(\eta-\xi)^2}{N}\sum_{\mathbf{k}}\left[2\eta\xi f_{\mathbf{k}}+(1-\alpha)g_{\mathbf{k}}^{+}-\frac{\eta\Gamma_{\mathbf{k}}^2}{R\Delta^2}g_{\mathbf{k}}^{-}\right],$$

$$B(\eta,\xi)=1+\frac{(\eta-\xi)^2}{N}\sum_{\mathbf{k}}\left\{2\eta^2 f_{\mathbf{k}}+\frac{\xi}{R}\left[(1+\alpha)^2-\frac{\Gamma_{\mathbf{k}}^2}{\Delta^2}\right]g_{\mathbf{k}}^{-}\right\},$$

where

$$f_{\mathbf{k}}=\frac{(1+\alpha)\Gamma_{\mathbf{k}}^2}{R^3\Delta^2}\left(\coth\frac{\Omega_+}{2\theta}-\coth\frac{\Omega_-}{2\theta}\right),$$

$$g_{\mathbf{k}}^{\pm}=\frac{1}{\theta}\left[(1-p)\sinh^{-2}\left(\frac{\Omega_+}{2\theta}\right)\pm(1+p)\sinh^{-2}\left(\frac{\Omega_-}{2\theta}\right)\right].$$

In the limit $\Delta\to\infty$ all the equations found within RPA go into the corresponding MFA equations. To find the spinodals on the phase diagrams it is necessary to solve the set of Eqs. (21) and (19). The obtained solutions give unambiguously the type of critical behavior and determine BCE and TCP.

Figures 3 and 4 represent $h-\theta$ and $\rho(\eta)-\theta$ phase diagrams at the same values of parameters. The lines of the equilibrium first-order phase transitions, which are generally referred to as the coexistence curves, were found with the

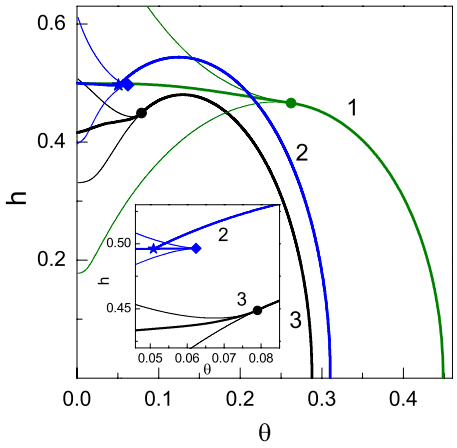

FIG. 3. (Color online) $h-\theta$ phase diagrams: (1) $\Delta=5$, $\alpha=0.8$; (2) $\Delta=5$, $\alpha=0.25$; and (3) $\Delta=1.5$, $\alpha=0.25$. Curves correspond to the equilibrium phase transition lines (thick) and the spinodals (thin). Full circle, diamond, and star denote the tricritical point, bicritical end point, and critical end point, respectively. Inset: an enlarged scale is used.

help of the Maxwell equal area construction,[32] and the spinodals were obtained from the set of Eqs. (19) and (21). On the $\rho(\eta)-\theta$ diagrams the coexistence curves enclose phase separated regions, and the spinodals outline the regions where $\partial\eta/\partial h<0$. Between a spinodal and coexistence curve the metastable homogeneous phases are possible.

As it is seen from Figs. 3 and 4 the system displays either tricritical or bicritical behavior depending on the values of parameters Δ and α. In the tricritical regime at fixed temperature $\theta<\theta_{\mathrm{TCP}}$ there exists only one liquid-solid phase transition of the first order [see Figs. 4(a) and 4(c)]. In the bicritical regime [see Fig. 4(b)] within a narrow temperature region between θ_{BCE} and θ_{CE} the system undergoes two

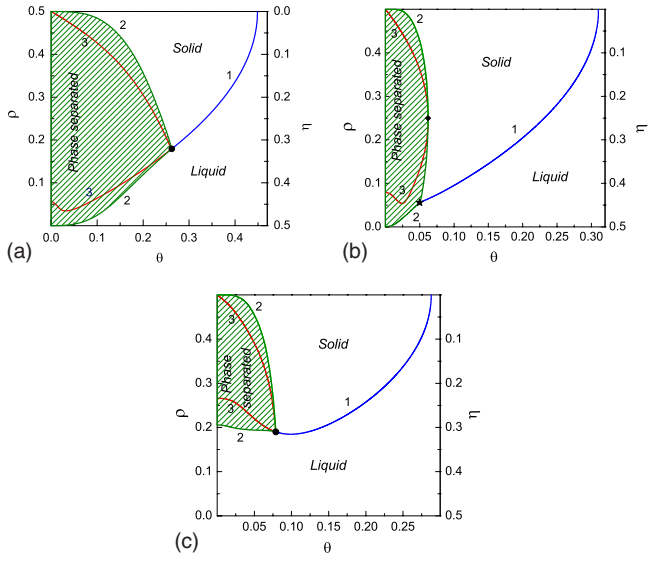

FIG. 4. (Color online) $\rho(\eta)-\theta$ phase diagrams: (a) $\Delta=5$, $\alpha=0.8$; (b) $\Delta=5$, $\alpha=0.25$; and (c) $\Delta=1.5$, $\alpha=0.25$. Solid lines are (1) the second-order liquid-solid transitions, (2) coexistence curves, and (3) spinodals. Full circle, diamond, and star denote the tricritical point, bicritical end point, and critical end point, respectively.

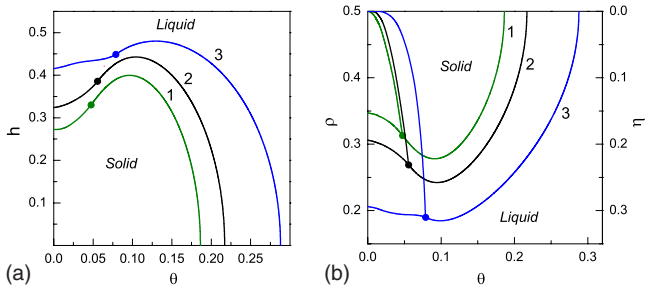

FIG. 5. (Color online) Phase diagrams (a) $h-\theta$ and (b) $\rho(\eta)-\theta$ at $\Delta=1.5$ and different α: (1) −0.1, (2) 0, and (3) 0.25. Full circles denote the tricritical points and solid curves indicate equilibrium transition lines.

phase transitions at fixed temperature: the liquid-solid second-order transition at low density and then, with increase in density, the first-order separation into two solid phases with different ρ. Below θ_{CE} in the bicritical regime only first-order liquid-solid transitions take place. Figure 3 demonstrates the same critical behavior of the system in the $h-\theta$ plane. Thus, it is seen that the hopping affects significantly the properties of the system. Mathematically, as compared to the MFA, the additional parameter Δ appears in the RPA equations. As a result, the transfer from one regime to the other can be performed not only by changing α, as it is within MFA, but also by changing Δ or both α and Δ. Figure 4 demonstrates the transformation of the bicritical regime into tricritical (a) with increase in α at fixed $\Delta=5$ as well as (c) with decrease in Δ at fixed $\alpha=0.25$. During these transformations CE and BCE shift along the coexistence curve approaching each other and eventually coincide turning into a TCP.

Figure 4 also illustrates another principal feature of the HCB related to the hopping contribution to the thermodynamics of the system. Namely, the high hopping (small Δ) results in retaining of the stable homogeneous liquid phase below TCP up to zero temperature. As the hopping decreases the liquid region at $\theta=0$ narrows and at a certain t vanishes. In the system with low hopping (large Δ) as temperature is decreased the homogeneous liquid of any density always separates into a liquid-solid mixture. In this regard the topology of the diagrams at large Δ becomes similar to that found within MFA.

The $h-\theta$ and $\rho(\eta)-\theta$ phase diagrams at $\Delta=1.5$ and different α are shown in Fig. 5. For all given α a continuous merging of the first- and second-order phase transition lines is seen at tricritical points indicated by full circles. The value of the tricritical temperature increases with α. From Fig. 5 also follows that in the HCB model without nnn interaction ($\alpha=0$) or with small nnn repulsion ($\alpha<0$) the first-order phase transitions take place at low temperatures, in contrast to the Ising model where at zero or small negative α only the second-order phase transitions are possible. If the nnn interaction is attractive ($\alpha>0$) or equal to zero ($\alpha=0$) then with decrease in temperature the solid phase becomes unstable at any density up to $\rho=0.5$ (the spinodal and coexistence curve have a common point $\theta=0$, $\rho=0.5$). If the nnn interaction is repulsive ($\alpha<0$) then there exists a density region near $\rho=0.5$ where the solid state, at least as metastable, persists up to $\theta=0$ (see Fig. 6).

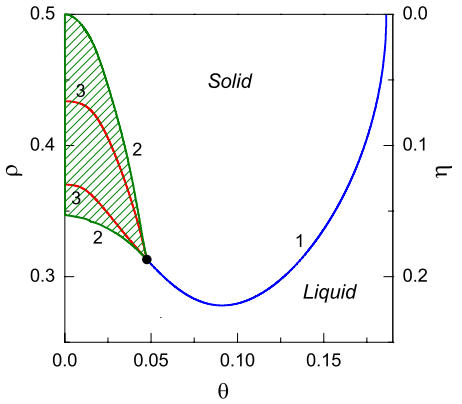

FIG. 6. (Color online) $\rho(\eta)-\theta$ phase diagram at $\Delta=1.5$ and $\alpha=-0.1$. Solid lines are (1) the second-order liquid-solid transition line, (2) coexistence curve, and (3) spinodal. Full circle denotes the tricritical point.

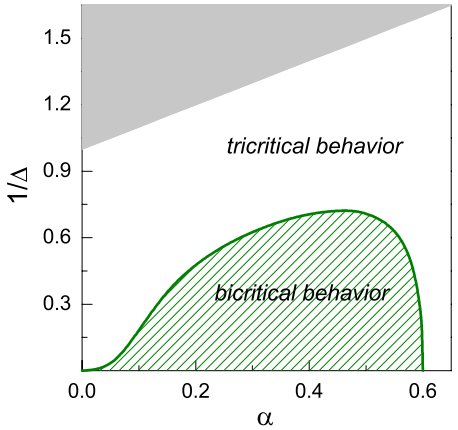

FIG. 8. (Color online) Regions of specific critical behavior of a square lattice HCB. The fill area is the region where $\Delta(1+\alpha)<1$ and only the liquid phase can exist.

An interesting feature of the obtained phase diagrams is the existence of reentrant transitions when with decrease in temperature the system passes sequentially from the paramagnetic (liquid) into antiferromagnetic (solid) phase, and then back into the paramagnetic (liquid) one. Such kind of transitions take place at both fixed h and fixed ρ. Temperature dependences of the total and sublattice magnetizations that indicate a reentrant phase transition are shown in Fig. 7. Note, that reentrant transitions for a square lattice HCB model at $\Delta=1.5$ with account for only nn interaction was found in Refs. 23 and 25 within quantum Monte Carlo simulations. The $h-\theta$ and $\rho(\eta)-\theta$ phase diagrams obtained here at $\Delta=1.5$, $\alpha=0$ are in a qualitative agreement with the results of Refs. 23 and 25.

The above results clearly demonstrate that the topology of the RPA diagrams and the type of the critical behavior depend significantly on the relationship between the hopping and interparticle interaction. The RPA provides a way for establishing the regions of bicritical and tricritical regimes as well as the critical line where one regime changes the other.

To do this we derive an equation for critical points where the spinodal branches meet. This equation follows from the condition that along the spinodal the total derivative of the left hand side of Eq. (21) over ξ is equal to zero. However, it is very cumbersome to be written out here in an explicit form. Solving the obtained equation together with Eqs. (19) and (21) at fixed Δ and α we determine a critical point which is of bi or tricritical kind depending on whether ξ is nonzero or zero. To find the line separating two regions of different critical behavior it is best to start with the bicritical region ($\xi>0$) at fixed α and then decreasing Δ to get the value $\xi=0$. The obtained point $\Delta(\alpha)$ lies on the sought critical line. Figure 8 shows the regions in the $\alpha-1/\Delta$ plane for $\alpha\geq 0$ where the HCB system demonstrates the critical behavior of different types. Fill area above the line $1/\Delta=1+\alpha$ specifies the region where only the liquid phase exists. In the MFA limit ($1/\Delta=0$) the system exhibits the bicritical behavior for $0<\alpha<0.6$ and tricritical one above $\alpha=0.6$ which is in accord with Ref. 30 (see also Sec. III). With increase in $1/\Delta$ the bicritical region gets narrow in α, so that its lower boundary shifts to the right and upper—to the left. Below $\Delta=\Delta_0\approx 1.378$ the region of bicritical regime vanishes, and from this point the system displays the tricritical behavior at any positive α. From Fig. 8 follows that the HCB with only nn interaction at any allowable finite Δ exhibits only tricritical behavior. Such is indeed the case in numerical calculations made for this model in Refs. 23–27.

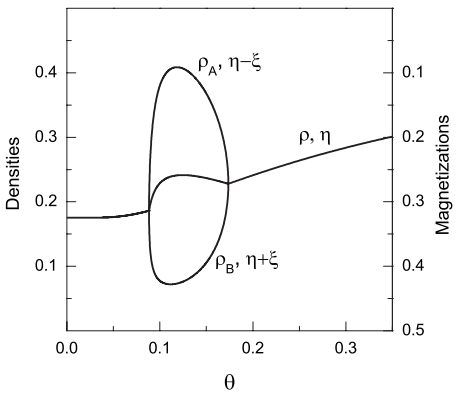

FIG. 7. Temperature dependences of total and sublattice densities (magnetizations) for $\Delta=1.5$, $\alpha=0.25$, and $h=0.46$.

V. THERMODYNAMICS WITHIN RPA

In this section we calculate the thermodynamic functions of the system under study. The internal energy per site $\mathcal{E}$ has the form

$$\mathcal{E}=\frac{\langle H_M\rangle}{J\gamma_0\Delta N}=\mathcal{E}_0-h\eta,$$

$$\mathcal{E}_0=-\frac{1}{2}\left(\frac{1}{\Delta}\langle S_{\mathbf{f}}^{+}S_{\mathbf{f}+\boldsymbol{\delta}}^{-}\rangle-\mathcal{K}\right),$$

where

$$\mathcal{K}=\langle S_{\mathbf{f}}^{z}S_{\mathbf{f}+\boldsymbol{\delta}}^{z}\rangle-\alpha<S_{\mathbf{f}}^{z}S_{\mathbf{f}+\boldsymbol{\gamma}}^{z}>. \tag{22}$$

Here $\langle\ldots\rangle$ denotes thermodynamic average and $<\cdots>$ combines thermodynamic and sublattice averages so that

$$< S^z_{\mathbf{f}} S^z_{\mathbf{f}+\boldsymbol{\gamma}} > = \frac{1}{2}(\langle S^z_{\mathbf{f}} S^z_{\mathbf{f}+\boldsymbol{\gamma}} \rangle_{\mathbf{f}\in A} + \langle S^z_{\mathbf{f}} S^z_{\mathbf{f}+\boldsymbol{\gamma}} \rangle_{\mathbf{f}\in B}).$$

Below we derive the exact relation connecting the internal energy of HCB with the Green function for transverse components of the spin operator. To do this we follow the procedure, set out in Ref. 33. As a first step, we substitute

$$S^z_{\mathbf{f}} = \frac{1}{2} - S^-_{\mathbf{f}} S^+_{\mathbf{f}} \tag{23}$$

into Eq. (22) and get

$$\mathcal{K} = \frac{1-\alpha}{4} - (1-\alpha) < S^-_{\mathbf{f}} S^+_{\mathbf{f}} > + \langle S^-_{\mathbf{f}} S^+_{\mathbf{f}} S^-_{\mathbf{f}+\boldsymbol{\delta}} S^+_{\mathbf{f}+\boldsymbol{\delta}} \rangle$$
$$- \alpha < S^-_{\mathbf{f}} S^+_{\mathbf{f}} S^-_{\mathbf{f}+\boldsymbol{\gamma}} S^+_{\mathbf{f}+\boldsymbol{\gamma}} > .$$

Then to find the averages of the products of four transverse spin operator components, we employ an exact equation of motion for the transverse Green function $\langle\langle S^+_{\mathbf{f}} | S^-_{\mathbf{f}'} \rangle\rangle$ and Eq. (23). Making use of the spectral relation for Green functions after some manipulations we get the required exact expression for the internal energy

$$\mathcal{E} = \frac{1}{4}\left[(1-\alpha)\eta - h(1+2\eta) - \frac{1}{\Delta}\langle S^+_{\mathbf{f}} S^-_{\mathbf{f}+\boldsymbol{\delta}} \rangle \right]$$
$$+ \frac{1}{N}\lim_{\varepsilon\to 0}\int_{-\infty}^{\infty} \omega n(\omega) \sum_{\mathbf{k}} \mathrm{Im}[G^{AA}_{\mathbf{k}}(\omega+i\varepsilon) + G^{BB}_{\mathbf{k}}(\omega+i\varepsilon)] d\omega,$$

where

$$n(\omega) = \left[\exp\left(\frac{\omega}{\theta}\right) - 1 \right]^{-1}.$$

Using Eqs. (15) and (16), after integration the internal energy within RPA takes the form

$$\mathcal{E} = \frac{1}{2}[(1-\alpha)\eta^2 - (1+\alpha)\xi^2] - \frac{1}{4\Delta}(1+2\eta)\langle S^+_{\mathbf{f}} S^-_{\mathbf{f}+\boldsymbol{\delta}} \rangle - h\eta,$$

where

$$\langle S^+_{\mathbf{f}} S^-_{\mathbf{f}+\boldsymbol{\delta}} \rangle = -\frac{\eta^2 - \xi^2}{N} \sum_{\mathbf{k}} \frac{\Gamma^2_{\mathbf{k}}}{R\Delta} \left(\coth\frac{\Omega_+}{2\theta} - \coth\frac{\Omega_-}{2\theta} \right).$$

Figure 9 demonstrates the temperature dependence of the heat capacity

$$C = \left(\frac{\partial \mathcal{E}}{\partial \theta}\right)_{\eta} = \frac{1}{J\gamma_0\Delta}\left[\frac{\partial}{\partial\theta}\left(\frac{\langle H_B \rangle}{N} + \mu\rho \right) \right]_{\rho}$$

in the case when the system undergoes two successive continuous phase transitions. It is clearly seen two λ points at the corresponding transition temperatures.

Figure 10 displays the magnetic susceptibility $\chi = \partial\eta/\partial h$ of the system in the paramagnetic phase as a function of temperature at different h. In the HCB language these dependences correspond to compressibility of the liquid state. It is seen that $\chi(\theta)$ demonstrates a distinct behavior according to whether h is higher or lower than a critical value h_c

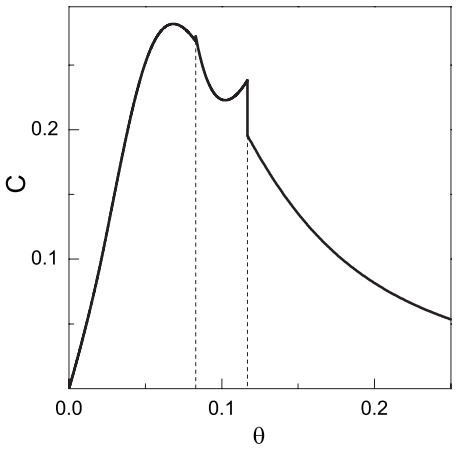

FIG. 9. Temperature dependence of the heat capacity per site at $\Delta=1.5$, $\alpha=0.25$, and $\rho=0.188$.

$$h_c = \frac{1}{2}\left(1 - \alpha + \frac{1}{\Delta}\right). \tag{24}$$

If $h > h_c$ the zero-temperature magnetic susceptibility $\chi(0) = 0$. With increase in temperature $\chi(\theta)$ increases passing through a maximum and then decreases approaching zero as θ tends to infinity. Such a behavior is quite similar to that found for an isotropic Heisenberg ferromagnet in an external magnetic field.[34,35] If $h < h_c$ the function $\chi(\theta)$ takes the finite value at $\theta=0$,

$$\chi_0 = \frac{1}{2h_c},$$

independent of the magnetic field. With increase in temperature the susceptibility drops from χ_0 to 0. The decrease in $\chi(\theta)$ is monotonic for all $h < h_c$ except the narrow region just below h_c, where the function demonstrates a nonmonotonic run: first, it rapidly decreases at small temperatures, passes a minimum then goes through a maximum after which monotonically decreases to zero. The physical reason for this be-

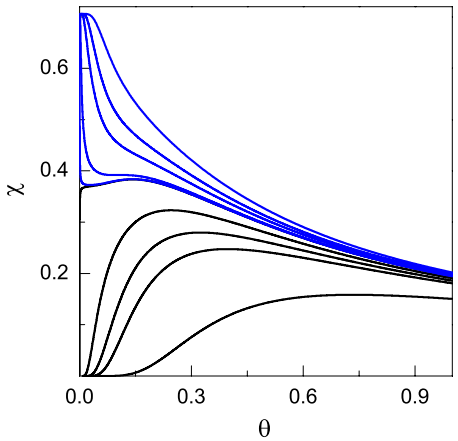

FIG. 10. (Color online) Temperature dependences of the magnetic susceptibility for $\Delta=1.5$, $\alpha=0.25$ in the paramagnetic phase at $h=0.5$, 0.6, 0.65, 0.7, 0.708, 0.7085, 0.8, 0.9, 1.0, and 1.5 (from top to bottom). The critical field $h_c = 17/24 = 0.708\ 33(3)$.

havior is a competition between the magnetic field h and anisotropy parameter Δ in the ordering of the spin system. Indeed, at high enough fields and low temperatures all the spins are directed along the magnetic field, the system is completely ordered ($\eta=0.5$), and the magnetic susceptibility obviously is equal to zero. In the case of small fields when the anisotropy parameter Δ prevails the magnetization η does not reach the maximal value of 0.5 even at $\theta=0$, and a zero-temperature magnetization is linear in h,

$$\eta(0) = \frac{h}{2h_c},$$

leading to a finite $\chi(0)=\chi_0$.

The critical field h_c is an essentially singular point for the magnetic susceptibility at $\theta=0$, which indicates the possibility of the phase transformations in the system. At $h=h_c$ a zero temperature gap in excitation spectrum $\Omega_-(\mathbf{k})$ Eq. (17) vanishes and then with decrease in field $\Omega_-(\mathbf{k})$ retains gapless up to the field when the transition into the antiferromagnetic state occurs. The value of h_c found from Eq. (24) at $\alpha=0$ coincides with the critical field H_{c2} following from the consideration of *XXZ* model with only nn interaction.[20,23,24] The field H_{c2} separates the region of spin-flop (SF) phase ($h<H_{c2}$) from the homogeneous paramagnetic state ($h>H_{c2}$) at zero temperature. Thus, Eq. (24) is the generalization of the upper field boundary for the existence of the SF phase at $\theta=0$ to the quantum HCB model with nn and nnn interactions
($\alpha\neq 0$). We also compared the field H_{c1}, at which the antiferromagnetic structure becomes unstable against spin-flop phase,[20,23,24] with the corresponding value found in the present work at $\alpha=0$ using the Maxwell equal area construction [see $h(0)$ in Fig. 5(a), curve 2]. It turned out that the field $h(0)\approx 0.32$ is less than the classical estimation for $H_{c1}\approx 0.37$ found in Refs. 20 and 24. This fact can be explained by an account for quantum fluctuations that make the spin system more compliant and thence reduce the critical field H_{c1}. On the other hand, $h(0)$ is very close to the value $H_{c1}\approx 0.31$ found within QMC simulations.[23] From Eq. (24) and Fig. 5 it follows that the region of SF phase at zero temperature narrows with increase in α.

It was found numerically[23–27] that a square lattice HCB model with nn interaction at a finite temperature undergoes a phase transition of Kosterlitz-Thouless type into a spin-flop state in which a long-range order is absent and the transverse correlators exhibit a powerlike decay at large distances. Despite the fact that RPA makes it possible to find upper and lower boundaries of SF phase at $\theta=0$, it is insufficient for interpretation of this phase at finite temperatures. The reason is that RPA gives unsatisfactory quantitative description of correlation functions at large distances,[34,35] and more advanced methods should be used.

Figure 11 shows the temperature dependences of the magnetic susceptibility of the system that undergoes phase transitions at constant h. Curve 1 represents the situation with only one second order phase transition whereas curve 2 corresponds to a reentrant phase transition when with decrease in temperature the system undergoes subsequently the second-order paramagnetic-antiferromagnetic transformation and then the first-order antiferromagnetic-paramagnetic one. Note that the reentrant transitions in the system always bring it to the disordered phase with the finite zero-temperature susceptibility χ_0.

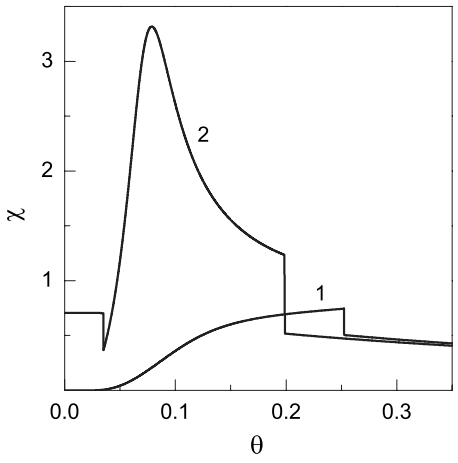

FIG. 11. Temperature dependences of the magnetic susceptibility at $\Delta=1.5$ and $\alpha=0.25$: (1) $h=0.3$ and (2) $h=0.43$.

VI. CONCLUSIONS

A square lattice hard-core boson model with nearest and next-nearest-neighbor interactions has been treated within the random phase approximation in terms of equivalent to it an anisotropic spin-1/2 *XXZ* model in a magnetic field. It is assumed that the nn interaction is repulsive while nnn interaction can be either attractive or moderate repulsive. The finite-temperature phase diagrams are built and thermodynamic functions of the system are calculated. Contrary to the widely used mean field approximation, the present method takes consistently into account the hopping term in the HCB Hamiltonian giving rise to the nontrivial dispersion of elementary excitations. The equation for the spinodal has been derived and studied in details for various values of the parameters. This equation also determines the type of critical points and their location on the phase diagrams. The behavior of the system has been investigated for different magnitudes of hopping t and ratio α ($\alpha>-0.5$) between the nn and nnn interactions.

The system under study undergoes the solid (antiferromagnetic)-liquid (paramagnetic) phase transitions that can be either of the first or second order and demonstrates two types of critical behavior. In the bicritical regime the first-order phase transition line on the $h-\theta$ diagram meets the line of the second-order phase transitions in a critical end point, then extends into the Néel solid phase ending inside it at a bicritical end point. In the tricritical regime the lines of the first- and second-order phase transitions join continuously at a tricritical point. The type of critical behavior is determined by the parameter α as well as the value of hopping t. We have shown that for HCB model with only nn interaction ($\alpha=0$) even arbitrary small hopping leads to the appearance of the first-order phase transitions in the low-temperature region, and the system is necessarily in the tricritical regime, whereas within MFA only continuous phase

transitions are possible in this case. In the present paper the connection of the hopping and the ratio between nn and nnn interactions with criticality of the system has been investigated. We have built within RPA the $\alpha - 1/\Delta$ diagram, the locus of critical points where bi and tricritical regimes change each other, for all positive α. It turned out that over the interval $1/(1+\alpha) < \Delta < \Delta_0 \approx 1.378$ only the tricritical regime is possible. At fixed $\Delta > \Delta_0$ two points $\alpha_{c1}(\Delta)$ and $\alpha_{c2}(\Delta)$ appear in the $1/\Delta - \alpha$ plane, so that inside and outside the interval $\alpha_{c1} < \alpha < \alpha_{c2}$ the system displays the bi and tricritical behavior, respectively. If $\Delta \to \infty$ then $\alpha_{c1}=0$ and $\alpha_{c2}=0.6$ in full agreement with the well-known MFA results.

The RPA analysis shows a significant distinction in the behavior of the HCB model at high and small hopping. Namely, at small hopping with decrease in temperature neither solid nor liquid can exist as stable homogeneous phases, so that below a definite temperature the system is necessarily separated into two-phase mixture. In this respect the system with small t displays behavior similar to that found for the Ising model at $\alpha > 0$. In the case of high enough hopping the properties of the system are quite different. Due to high kinetic energy there exists a density region where a stable homogeneous liquid phase occurs up to zero temperature. Furthermore, if the nnn interaction is repulsive then the density region of absolute instability at $\theta=0$ extends till some $\rho = \rho_0 < 0.5$. As a result, above ρ_0 a homogeneous solid phase can exist up to zero temperature at least as metastable.

Our investigations indicated conclusively the possibility of reentrant phase transitions in a square lattice HCB with nn and nnn interactions. In particular, we confirm the corresponding numerical results[23–25] found for HCB with only nn interaction at $\Delta = 1.5$.

Thermodynamic properties of the system under study are investigated. For the anisotropic 1/2-spin *XXZ* model in a magnetic field we have derived the exact expression connecting the internal energy with the transverse Green function. The heat capacity and magnetic susceptibility are calculated within RPA. As one would expect, the dependences $C(\theta)$ and $\chi(\theta)$ exhibit λ point kind irregularities at the corresponding phase transition temperatures. In the paramagnetic phase a temperature run of the susceptibility depends significantly on whether the magnetic field h is lower or higher than the critical value h_c which is a function of both α and Δ. The quantity h_c is the critical field that determines the phase transition between spin-flop and paramagnetic states at zero temperature. A detailed investigation of the SF phase at zero temperature will be a subject of a separate publication.

[1] R. T. Whitlock and P. R. Zilsel, Phys. Rev. **131**, 2409 (1963).
[2] T. Matsubara and H. Matsuda, Prog. Theor. Phys. **16**, 569 (1956).
[3] H. Matsuda and T. Tsuneto, Prog. Theor. Phys. **46**, 411 (1970).
[4] T. Siller, M. Troyer, T. M. Rice, and S. R. White, Phys. Rev. B **63**, 195106 (2001).
[5] A. Dorneich, W. Hanke, E. Arrigoni, M. Troyer, and S. C. Zhang, Phys. Rev. Lett. **88**, 057003 (2002).
[6] A. P. Kampf and G. T. Zimanyi, Phys. Rev. B **47**, 279 (1993).
[7] G. G. Batrouni, B. Larson, R. T. Scalettar, J. Tobochnik, and J. Wang, Phys. Rev. B **48**, 9628 (1993).
[8] M.-C. Cha, M. P. A. Fisher, S. M. Girvin, M. Wallin, and A. P. Young, Phys. Rev. B **44**, 6883 (1991).
[9] E. S. Sørensen, M. Wallin, S. M. Girvin, and A. P. Young, Phys. Rev. Lett. **69**, 828 (1992).
[10] E. Altman, W. Hofstetter, E. Demler, and M. D. Lukin, New J. Phys. **5**, 113 (2003).
[11] R. T. Scalettar, G. G. Batrouni, A. P. Kampf, and G. T. Zimanyi, Phys. Rev. B **51**, 8467 (1995).
[12] G. G. Batrouni, R. T. Scalettar, G. T. Zimanyi, and A. P. Kampf, Phys. Rev. Lett. **74**, 2527 (1995).
[13] G. Murthy, D. Arovas, and A. Auerbach, Phys. Rev. B **55**, 3104 (1997).
[14] S. Wessel and M. Troyer, Phys. Rev. Lett. **95**, 127205 (2005).
[15] T. N. Antsygina, I. I. Poltavsky, K. A. Chishko, T. A. Wilson, and O. E. Vilches, Low Temp. Phys. **31**, 1007 (2005).
[16] T. N. Antsygina, I. I. Poltavsky, and K. A. Chishko, Phys. Rev. B **74**, 205429 (2006).
[17] I. Bloch, J. Dalibard, and W. Zwerger, Rev. Mod. Phys. **80**, 885 (2008).
[18] A. Micheli, G. K. Brennen, and P. Zoller, Nat. Phys. **2**, 341 (2006).
[19] T. Lahaye, C. Menotti, L. Santos, M. Lewenstein, and T. Pfau, arXiv:0905.0386 (unpublished).
[20] D. P. Landau and K. Binder, Phys. Rev. B **24**, 1391 (1981).
[21] H. J. Herrmann and D. P. Landau, Phys. Rev. B **48**, 239 (1993).
[22] F. Hébert, G. G. Batrouni, R. T. Scalettar, G. Schmid, M. Troyer, and A. Dorneich, Phys. Rev. B **65**, 014513 (2001).
[23] G. Schmid, S. Todo, M. Troyer, and A. Dorneich, Phys. Rev. Lett. **88**, 167208 (2002).
[24] M. Holtschneider, W. Selke, and R. Leidl, Phys. Rev. B **72**, 064443 (2005).
[25] M. Holtschneider, W. Selke, and S. Wessel, Phys. Rev. B **75**, 224417 (2007).
[26] W. Selke, M. Holtschneider, R. Leidl, S. Wessel, and G. Bannasch, in *Computer Simulation Studies in Condensed Matter Physics XXI*, edited by D. P. Landau, S. P. Lewis, and H. B. Schuttler (Springer-Verlag, Heidelberg, Berlin, in press).
[27] W. Selke, G. Bannasch, M. Holtschneider, I. P. McCulloch, D. Peters, and S. Wessel, in *Condensed Matter Physics* (in press).
[28] L. Dang, M. Boninsegni, and L. Pollet, Phys. Rev. B **78**, 132512 (2008).
[29] K. Motizuki, J. Phys. Soc. Jpn. **14**, 759 (1959).
[30] J. M. Kincaid and E. G. D. Cohen, Phys. Rep. **22**, 57 (1975) and references therein.
[31] S. V. Tyablikov, *Methods in the Quantum Theory of Magnetism* (Plenum Press, New York, 1967).
[32] K. Huang, *Statistical Mechanics* (Wiley, New York, 1963).
[33] W. Gasser, E. Heiner, and K. Elk, *Greensche Funktionen in Festkörper- und Vielteilchenphysik* (Wiley-VCH Verlag, Berlin, 2001).
[34] T. N. Antsygina, M. I. Poltavskaya, I. I. Poltavsky, and K. A. Chishko, Phys. Rev. B **77**, 024407 (2008).
[35] I. Junger, D. Ihle, J. Richter, and A. Klümper, Phys. Rev. B **70**, 104419 (2004).